Dual confinement of sulphur with rGO-wrapped microporous carbon from β-cyclodextrin nanosponges as a cathode material for Li–S batteries

Zubair, Usman; Anceschi, Anastasia; Caldera, Fabrizio; Alidoost, Mojtaba; Amici, Julia; Francia, Carlotta; Zanetti, Marco; Trotta, Francesco; Bodoardo, Silvia; Penazzi, Nerino. Dual confinement of sulphur with rGO-wrapped microporous carbon from β-cyclodextrin nanosponges as a cathode material for Li–S batteries. JOURNAL OF SOLID STATE ELECTROCHEMISTRY. None pp: 1-10.
DOI: 10.1007/s10008-017-3664-6

Dual confinement of sulphur with rGO wrapped microporous carbon from β-cyclodextrin nanosponges as a cathode material for Li-S batteries.

Usman Zubair[1], Anastasia Anceschi[2], Fabrizio Caldera[2], Mojtaba Alidoost[1], Julia Amici[1], Carlotta Francia[1], Marco Zanetti[2], Francesco Trotta[2], Silvia Bodoardo[1], Nerino Penazzi[1].*

[1]Department of Applied Science and Technology, (DISAT), Politecnico di Torino, C.so Duca degli Abruzzi 24 - 10129 Torino – (ITALY).

[2]Department of Inorganic Chemistry, Physical Chemistry and Chemistry of Materials, Università degli Studi di Torino, Via Pietro Giuria 7 - 10125 Torino – (ITALY)

**Corresponding author. Tel.: +39 011 090 4641; fax: +39 011 090 4699.*

**E-mail address: silvia.bodoardo@polito.it*

Abstract

A novel approach was developed to synthesize microporous carbon spheres with pores size ranges from 5-11 Å from hyper cross-linked polymer β-cyclodextrin. Sulphur was incorporated in the micropores by solution impregnation followed by melt infusion. The resultant carbon sulphur (C/S) composite was wrapped in reduced graphene oxide (rGO) to provide conductive pathways to access the sulphur in micropores and protect the surface adhered sulphur. The cathode material obtained from rGO wrapping showed an initial discharge capacity of 1103 mA h g^{-1} at 0.1 C, maintaining a capacity of 626 mA h g^{-1} at 0.2 C with capacity loss of 0.14 % per cycle for more than 100 cycles. In another cell configuration using carbon paper as an interlayer, discharge capacity raised to 850 mA h g^{-1} at 0.2 C and maintained it for 100 cycles with excellent rate capability and high Coulombic efficiency. The good performance may be referred to excellent conductive networks, porous architecture of carbon spheres and adsorption of catholyte by fibrous interlayer that can effectively reduce the polysulfide shuttling.

Keywords: Microporous Carbon, Lithium Sulphur battery, rGO wrapping, Dual confinement

1. Introduction

The future of portables devices, electric vehicles and smart grids demand long life and high energy density batteries. State of art Li ion batteries are limited in terms of gravimetric capacity energy density (~300 W h kg^{-1}) and, being a mature technology, it is not to be expected any marked improvement of the performance [1]. Li/S batteries – a post Li ion technology – provide a sound

answer to such requests, as they offer high theoretical capacity (1675 Ah kg^{-1}) [2]. Theoretically, the S cathode can deliver a specific energy of 2600 W h kg^{-1}, about five times higher than those of available insertion-materials of Li-ion batteries at a significantly lower cost [3]. The development of Li/S system faces several challenges such as low degree of sulphur utilization, gradual capacity fading, poor rate capability and low Coulombic efficiency mainly due to low conductivity of S_8 (5×10^{-30} S cm^{-1}), solubility of intermediate polysulphides, shuttling of polysulphides and lack of morphology restoration at electrode reoxidation [4]. S_8 cathode usually discharges in two plateaus; one plateau appears at a voltage (~2.3 V vs. Li^+/Li) in which S_8 reduced to S_8^{2-} to S_4^{2-}, a second long plateau approximately at 2.1 V vs. Li^+/Li related to transformation of Li_2S_4 to Li_2S_2 and at last low conductivity Li_2S formation. Lithium polysulphides (PS) (Li_2S_n, n = 4−8) are soluble in the liquid electrolyte and cause the shuttle phenomenon. The final reduced product of S_8 is Li_2S that is itself insoluble and poorly conductive [5]. Cathode design approaches aim at achieving complete confinement of sulphur, without downgrading the practical properties of the cell, mainly the gravimetric and volumetric energy densities. The active sulphur materials have to be well embedded into the conducting matrices. In this regard, carbon is considered an optimal material for its lightweight and conductive nature, but it can also act as a framework to encapsulate the redox products [3]. In literature, sulphur appears to have been housed into various carbon structures such as micro [6-8], meso [5, 9, 10] and macroporous [11] carbons, carbon nanotubes [8, 12, 13], carbon fibres [14] and graphene [13, 15-17] and functional materials have been synthesized to answer the limitations linked with Li-S system. In previous studies [18, 19], mesoporous carbons were suggested extensively as ideal candidates to host sulphur inside the pores and avoid solubilisation of PS into electrolyte. Since mesoporous structures still exhibit an open structure, complete immobilization of polysulphides is not achievable as the system is well in contact with the electrolyte that causes gradual degradation of capacity [20]. Macroporous and microporous carbons were least considered because of lower PS entrapment capabilities of macropores owing to relatively open structure [18], and lower sulphur hosting capacities of micropores due to very small pores dimensions. In a very few studies, microporous carbon matrices were investigated comprising the pores size around 0.5 nm, those that can solely accommodate short-chain sulfur species (predominately S_2) and metastable sulfur allotropes $S_{2–4}$ via confining them in carbon micropores [7, 12, 21]. Small $S_{2–4}$ molecules showed excellent electrochemical performance and different electrochemical responses from the traditional S_8

material. A solid-solid mechanism of lithiation/delithiation reactions of the small $S_{2–4}$ molecules was suggested [21], although it has been recently reported that small S molecules in the micropores of carbon matrices is not a necessary condition such that this mechanism is realized. [22] Microporous carbon were either obtained by means of templating [23] or by pyrolysis of biomass [24] but Ryu *et al.* [25] had shown that it is possible to achieve high capacity sulphur cathode using solution impregnation only. Others reported ball mixing, melt infusion, and vapour phase diffusion to achieve homogenous impregnation of sulphur into the pores [5, 8, 10]. Wrapping of carbon sulphur composites in various conductive polymers such as polyaniline and in conductive carbon matrices as graphene sheets was also realized with some success [19, 26, 27]. A promising strategy for the development of high-performance Li-S batteries relies on both S_8 and $S_{2–4}$ incorporation. In this work, we have considered the caging of small S allotropes in microporous conductive matrices to reduce polysulphides solubility while increasing the cathode electronic conductivity. A sustainable solution is the production of conductive microporous carbon matrices from bio-based materials. Here, microporous carbons with a wide range of pore size distribution are synthesized by carbonizing β-cyclodextrin nanosponges. Sulphur is then incorporated via solvent impregnation and thermal infusion [28]. As to better retain the active sulphur mass upon reduction/oxidation when highly soluble lithium polysulphides are formed, a dual protection is achieved. To address this issue, we explored the idea [19] of graphene-coated the carbon/sulphur composites. Thanks to carbon hydrophobicity, we directly wrapped the C/S composite with reduced graphene oxide (rGO), to access and dually protect the sulphur inside the micropores of the carbon matrix [29]. Thus, high sulphur utilization is guaranteed. Additionally, rGO wrapping provides the electrode of sufficient flexibility to bypass sulphur volume expansion/contraction during electrochemical cycling and reduces polysulphide shuttle effects.

2. Experimental Section

As mentioned, sulphur is confined in the microporous carbon spheres, derived from pyrolysis of hyper cross-linked polymer β-cyclodextrin, by solution impregnation followed by melt infusion. The as prepared carbon-sulphur composite is then wrapped with reduced graphene oxide (rGO) to access and dually protect the sulphur inside the micropores of the carbon matrix. A sketch of the

strategy implemented to synthesize the C/S composite materials with rGO wrapping is reported in the scheme 1.

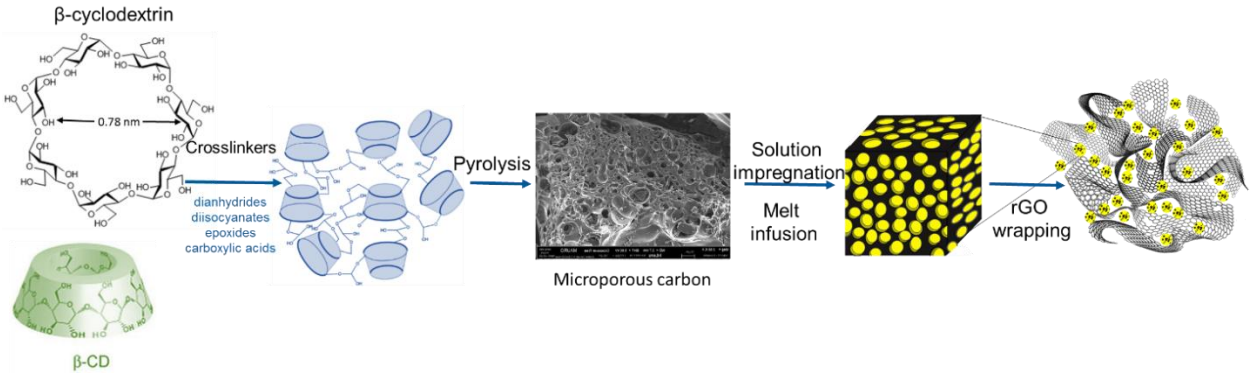

Scheme 1: Schematic representation of the opted strategy to prepare rGO wrapped functional microporous C/S composites.

2.1. Materials Preparation

Synthesis of microporous carbon spheres: Polymer β-cyclodextrin also termed as β-cyclodextrin nanosponge was prepared by crosslinking reaction using pyromellitic dianhydride (PY) following a procedure previously described [30]. The PY cross-linked NS were prepared in 1:4 molar ratio of β-CD and PY. 11.35 g of anhydrous β-CD (10.0 mmol) (Roquette Italia SpA) and 17.45 g of PY (80.0 mmol) (Sigma Aldrich) were dissolved in 100 mL of dimethyl sulfoxide (DMSO) (Fluka) containing 2.7 mL trimethyl amine (19.4 mmol) (Sigma Aldrich) and were allowed to react at room temperature for 3 h. Once the reaction was complete, the solid was grounded in a mortar and Soxhlet extracted with acetone for 24 h. This PY β-cyclodextrin nanosponge was then pyrolysed at 800 °C with heating rate of 10 °C/min in nitrogen gas flux for 2 hours [31] to obtain microporous carbon (**MPC**) as shown in scheme 2.

Preparation of C/S composites: 1.5 g of sulphur (Sigma Aldrich) are dissolved in DMSO at 90 °C. 1 g of MPC is added in the solution mixture under heating. Continuous heating of the mixture for 6 hours under magnetic stirring was carried out to impregnate the MPC. The mixture is cooled down to room temperature to crystallize the sulphur in the spongy structure of carbon. The solution impregnated C/S composite (**SI_CS**) is collected by centrifugation. The washing of the composite is carried out using ethanol. Then, SI_CS is transferred to furnace tube under Argon stream, where

the composite is heated to 115 °C for 6 hours. The temperature is then raised to 155 °C for 12 hours. The melt infused C/S composite (**MI_CS**) is crushed into powder using pestle and mortar.

Wrapping of C/S composite into rGO: 0.14 g of graphene oxide (GO) (Graphena) is reduced at 700 °C for 2 hours under H_2/Ar atmosphere. The resultant 0.06 g of reduced graphene oxide (rGO) was well dispersed in 100 ml ethanol using sonication. 1 g of MI_CS is dispersed in rGO ethanol solution under magnetic stirring for 5 hours. Then, temperature is raised to 80 °C to evaporate ethanol. On removing the heat, the whole dispersion settles down quickly, which proves that rGO is adhered to the surfaces of MI_CS composite. Ethanol was spewed out from the top of rGO wrapped MI_CS composite (**rGO@MI_CS**). rGO@MI_CS composite is vacuum dried at 60 °C for 8 hours.

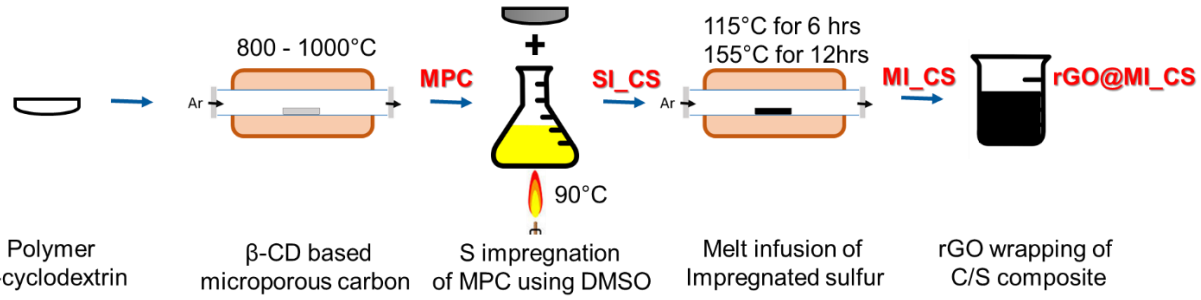

Scheme 2: Schematic illustration of the production steps to prepare rGO functional microporous C/S composites

2.2. Materials Characterization

The morphology of the synthesized MPC and the as obtained C/S composites was examined using field-emission scanning electron microscopy (FESEM, JEOL-JSM-6700F). Energy dispersive X-ray spectroscopy (EDS) of the composites was also performed using JEOL-JSM-6700F to investigate the sulfur presence into the structure of carbon sponge. Sulphur mapping is acquired under FESEM by imaging the X-ray signals from composite surface. The porous structures of MPC and C/S composites were analysed by recording nitrogen adsorption isotherms at 77 K by exposing at a series of precisely controlled pressures from 0 to 1 with an ASAP 2020 Instrument (Micromeritrics). Prior to the adsorption measurements, the MPC and C/S composites were degassed at 150 °C and 50 °C (to avoid the sublimation of the sulphur) respectively under vacuum (10 μm Hg) for 12 h to remove the adsorbates and residual moisture, and then sample

were cooled to nitrogen cryogenic temperature (77K). The specific surface area (SSA) of the samples was calculated by Brunauer–Emmett–Teller (BET) method using Langmuir model within the relative pressure range of 0 to 1 and the micropore volume and pore size distribution were estimated using density functional theory (DFT) assuming a slit geometry of the pores. The elemental analysis was carried out using a Flash EA 1112 series CHNS/O Analyzer (Thermo Scientific). The samples were weighed in Tin capsules, placed inside the instrument, and then dropped into an oxidation/reduction reactor maintained at 900-1000 °C. All the organic and inorganic substances are converted into elemental gases that, after further, reduction are separated in a chromatographic column and finally detected. The XRD patterns were recorded on a Panalytical X'Pert PRO diffractomer with a PIXcel detector, using Cu Ka radiation, under the conditions of 2θ = 10-100° and 2θ step size = 0.03, to observe the presence of sulphur.

2.3. Electrochemical measurements

Cells were assembled in Ar-filled dry glove box (Mbraun Labstar) using an ECC-STD electrochemical cell configuration (EL-Cell, Gmbh). The geometric area of the electrodes was 2.54 cm^2. The cathode contained the different S/C composite materials above described. A lithium disc (18 x 0.2 mm, Chemetall s.r.l.) was used as the anode. A Celgard EH2010 (trilayer PP/PE/PP) and glass fibre 18 mm x 0.65 mm saturated in the electrolyte was used as the separator. In other cell configuration, glass fibre separator is replaced by carbon fibre paper (GDL, SIGRACET GDL-24BC, SGL Technologies) to adsorb catholyte. The electrolyte consisted of 1,2-dimethoxyethane (DME) and 1,3-dioxolane (DIOX) 1:1 (v/v) with 1 M lithium trifluoromethanesulfonate ($LiCF_3SO_3$, LiTFSI) and 0.25 M $LiNO_3$. Cells were galvanostatically discharged by an Arbin BT-2000 battery tester at room temperature. Cycling tests were performed with 1^{st} 5 cycles discharge to 1.8 V and charge to 2.6 V at C/10. Onward cycling was carried out between 1.8 V and 2.6 V at C/5. The C-Rate is calculated using a theoretical capacity of 1672 mA h g^{-1}.

3. Results and Discussion

3.1. Synthesis and Characterization:

Morphologies of functional β-cyclodextrin MPC spheres and the as obtained sulphur composites were analysed by FESEM. **Figure 1** reveals interesting structural and textural properties of MPC from β-cyclodextrin nanosponge. MPC exhibits a spongy structure that makes it absorptive for sulphur. Sulphur shows a strong adsorbate-adsorbent interaction and can be chemisorbed in

functional microporous carbon at higher temperature [32]. **Figure 2** depicts the morphologies of SI_CS, MI_CS, and rGO@MI_CS. FESEM of SI_CS shows that sulphur (light grain in **Fig. 2a**) is homogeneously distributed on the surface of MPC, but sulphur is appeared as big clusters, those are loosely adsorbed at the surface. As concern the carbon micropores, given that the pore size of microporous carbons is less than the dimensions of cyclo-S_8, the ring-like configuration cannot be maintained, and sulphur can only be stored as chain-like sulphur molecules [12]. Thus, it is not possible for S_8 crystals to penetrate inside micropores because of larger dimension as S_8 crystals mostly occur in either orthorhombic α-sulfur form with sixteen S_8 molecules within unit cell or monoclinic β-sulfur with six S_8 molecules [33]. FESEM micrograph of MI_CS (**Fig. 2b**) shows negligible sulphur presence on the surface. Actually, sulphur melts at 115 °C but at a little higher temperature 155 °C it shows the minimum viscosity (0.066 poise) [34] and starts degrading into lower molecular metastable allotropes such as S_6, S_4, S_3, and S_2 [35]. It is believed that physical confinement of smaller species in micropores let the smaller allotropes to exist in primitive form through discharging and charging cycling. FESEM image of rGO@MI_CS (**Fig. 2c**) shows the morphology of the sulphur carbon composite wrapped with rGO. The planar structures typical of graphene sheets can be clearly observed, which are perpendicular to the plane, randomly crumpled and interconnected, forming a disordered solid. It can be observed that CS particles are very well wrapped by rGO, this was achieved by well dispersion of rGO and MI_CS in ethanol under sonication and, complete clearing out of dispersion on heating at 80 °C. rGO solubility in ethanol is around 0.91 μg ml^{-1} with stable dispersion at room temperature [36], but during synthesis there was an immediate disappearance of rGO from ethanol on removing heat and stirring. Therefore, it can be inferred that rGO has very good hydrophobic interaction with MPC particles.

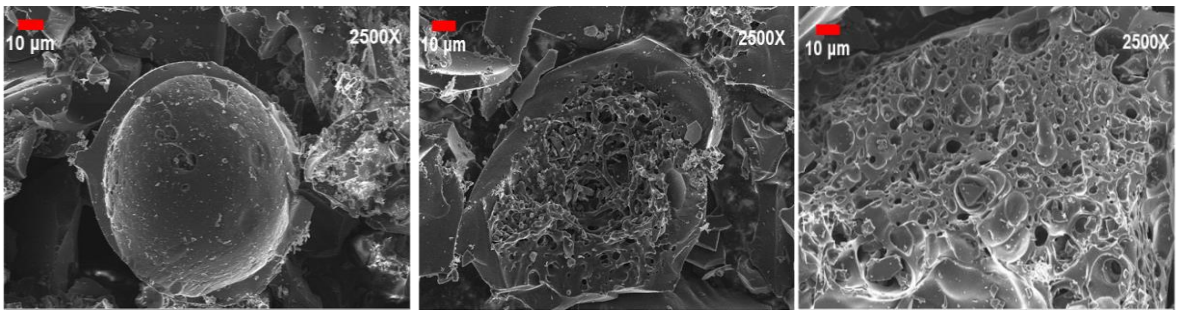

Figure 1: FESEM images of MPC prepared from β-cyclodextrin nanosponge

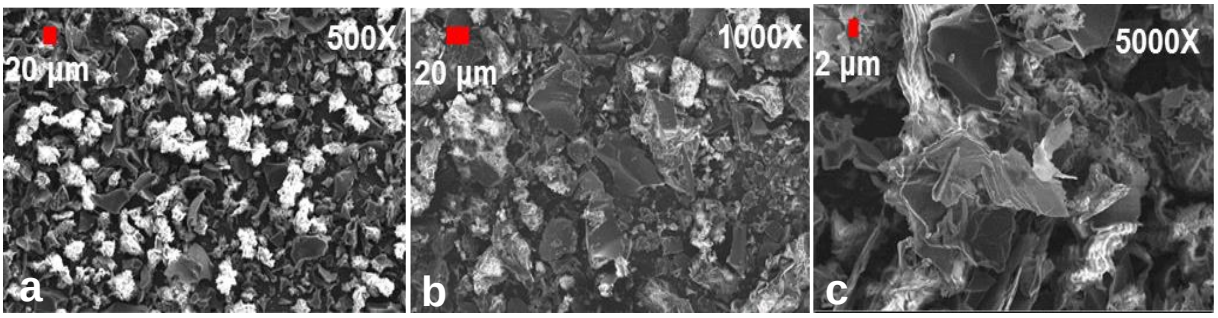

Figure 2: SEM images of **a)** SI_CS **b)** MI_CS **c)** rGO@MI_CS (images are at different scale to observe the typical structures present in the composites)

Absence of contrast in the back scattered FESEM image of rGO@MI_CS (**Fig. 3c**) is the evidence of appropriate wrapping by rGO sheets. These two images show undistinguishable difference in morphology because of the CS composite resides inside rGO as expected.

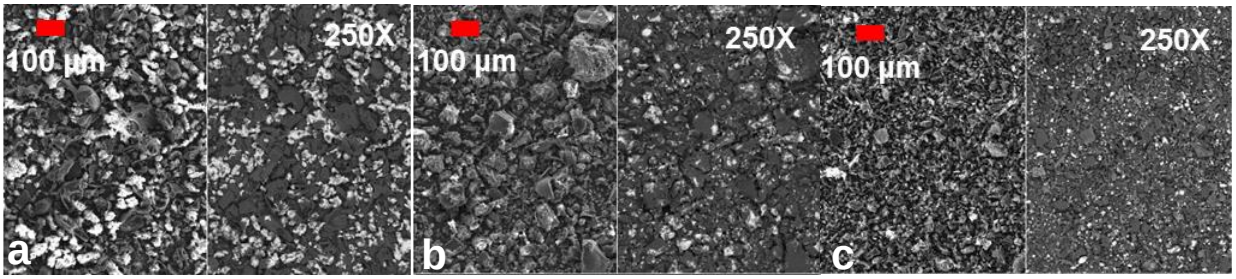

Figure 3: Secondary image and back-scattered contrast of carbon and sulfur **a)** SI_CS **b)** MI_CS **c)** rGO@MI_CS

The SEM-EDS elemental mappings were performed to characterize the presence of sulphur in the carbon matrices. In **Fig. 4a**, big sulphur clusters are present over or at the same level as the carbon material grains. In both the composites MI_CS (**Fig. 4b**) and rGO@MI_CS (**Fig. 4c**), sulphur can be detected as diffused in the structure with a minor amount of sulphur inside the fractures of the surface. In rGO@MI_CS, the carbon seems prevailing and sulphur is diffused in the network, which indicates that sulphur at the CS surface is also wrapped by rGO sheets.

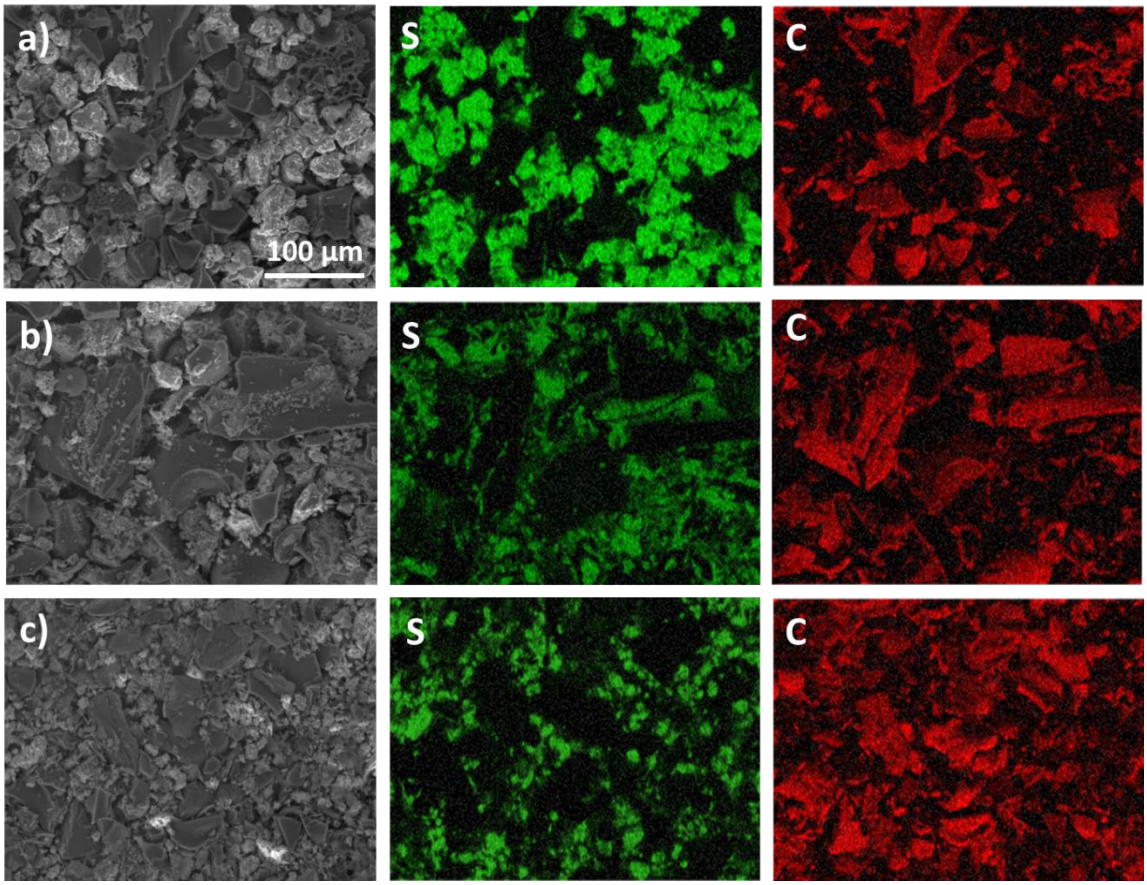

Figure 4: Sulphur mapping in C/S composites using EDS analysis for **a)** SI_CS **b)** MI_CS **c)** rGO@MI_CS

Elemental analysis of MPCs showed that the carbon content was 78 wt. % with non-negligible amounts of O no sulphur is present as depicted in **Table 1**. While the elemental analysis of C/S composites revealed a sulphur content around 63 wt. %, 59 wt. % and 49 wt. % for SI_CS, MI_CS and rGO@MI_CS, respectively as shown in Table 1.

Table 1: Elemental analysis of MPC and C/S composites

Sample	% N	% C	% H	% S	%O evaluated
MPC	1.26	78.13	0.69	0.00	19.92
SI_CS	0.65	39.17	0.34	62.41	0.00
MI_CS	0.81	42.62	0.26	58.43	0.00

rGO@MI_CS	0.59	46.30	0.83	48.27	3.99

The carbon obtained after the pyrolysis process was characterized by nitrogen adsorption-desorption isotherms. The result exhibited type I isotherm according to IUPAC classification that is the characteristic of microporous materials. MPC showed a specific surface area of 560 $m^2 g^{-1}$, with average pore volume of 0.15 $cm^3 g^{-1}$ and average pore diameter 5-13 Å as shown in the **Fig. 5**. Contrary, the C/S composite showed very poor adsorption behaviour, SI_CS, MI_CS and rGO@MI_CS exhibited the specific area 11.24 $m^2 g^{-1}$, 17.45 $m^2 g^{-1}$ and 12.32 $m^2 g^{-1}$ respectively. The embedding of sulphur into the carbon spheres contributes to such a significant decrease of the surface area, due to a strong adsorption and retention of elemental sulphur [37]. According to Liang *et al.* [38] when sulphur is loaded the micropores of an activated mesoporous carbon through a solution infiltration method the micropore volume is completely filled up when the sulphur loading is above 37.1 wt %. In particular, this is consistent with the FESEM images of SI_CS (**Fig. 2a and 3a**), which indicate a serious surface deposition and aggregation of sulphur over the carbon surface.

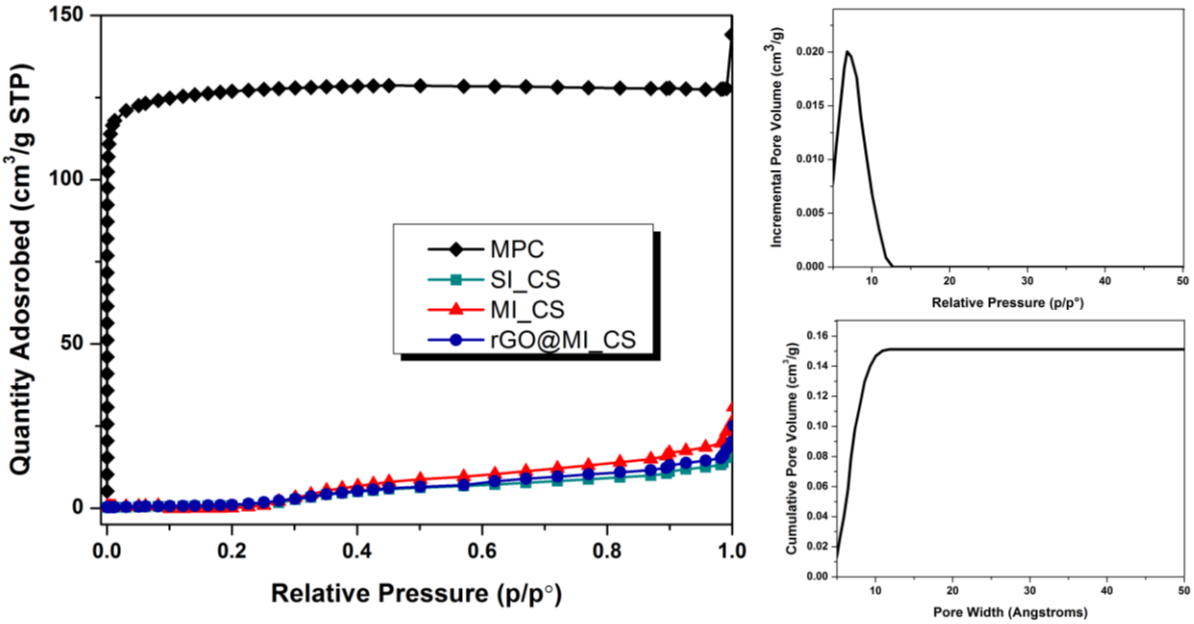

Figure 5: Isotherms from BET analysis of a) MPC b) SI_CS c) MI_CS d) rGO@MI_CS

Fig. 6a exhibits the XRD patterns of pristine sulphur, MPC and C/S composites. The sharp diffraction peaks denote that sulphur exists in a crystalline state, while the broad diffraction around

24° in the MPC pattern indicates the amorphous characteristic of carbon spheres. It can be highlighted that XRD pattern for SI_CS closely resembles to that of pristine sulphur without any effect from amorphous peaks of MPC. In contrast, MI_CS and rGO@MI_CS showed the amorphous peak of MPC along with sulphur peaks that illustrate that most of the sulphur is now diffused into micro and macropores of the carbon material. Such a highly dispersed state may also result in the improvement of the electric conductivity of the composite cathode. For a comprehensive characterization of C/S composite, a sketch of the MI_CS with rGO synthesized material is provided in **Fig. 6 b**, which depicts the distribution of sulphur in the porous network. It is noteworthy that without performing any post treatment after melt infusion, it is not possible to get rid of sulphur on the surfaces. Indeed, S melt infusion in a microporous carbon is generally accompanied by post thermal treatments to vaporize the superfluous sulphur on the outer surface of carbon spheres [37]. Here, the idea is to store such sulphur inside rGO so as it becomes available for the electrochemical reaction, limiting its dissolution as much as possible during cell cycling. In this case, wrapping of MI_CS with rGO can mask the sulphur present on the surfaces, thus provide the conductive pathways and hinder the polysulfide dissolution.

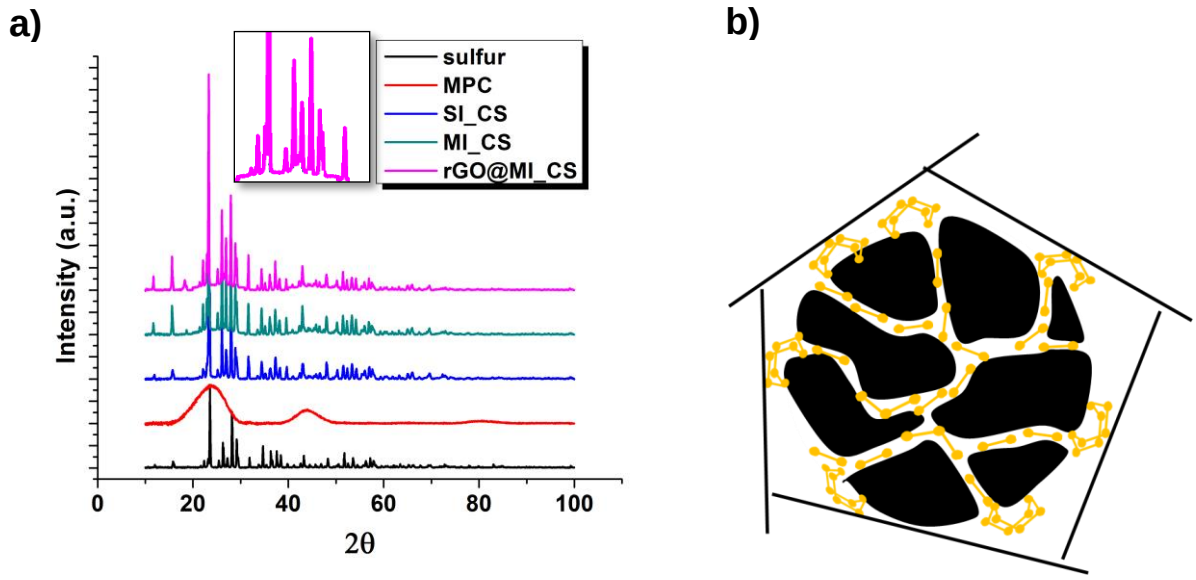

Figure 6: a) XRD analysis of sulphur, carbon and carbon sulphur composite **b)** illustration of sulphur distribution in rGO wrapped microporous carbon from the characteristics EDS, XRD and BET results.

3.2. Electrochemical Performance:

As observed in **Fig. 7 a**, the 1st discharge capacity at 0.1C of SI_CS cathode is about 510 mA h g^{-1}. The characteristic two plateaus on discharge are merely distinguishable and the cathode retains only about 60% of the initial discharge capacity at the 2nd discharge. Such behaviour can be ascribed to sulphur mainly existing on the surface of MPC, which fast dissolves into electrolyte as PS. Two plateaus at 2.3 and 2.1 V are clearly distinguishable in the voltage profile of MI_CS, **Fig. 7 b**. The first voltage plateau is consistent with the reaction from S_8 to S_4^{2-}, which is mostly due to cyclo-S_8 located on the carbon surface. The second voltage plateau arises from conversion of S_{2-4}, the latter mostly confined in the carbon micropores. Higher capacity retention is observed in this case, as the initial discharge capacity of MI_CS is 842 mA h g^{-1} and 610 mA h g^{-1} at the 2nd discharge at 0.1 C. Sulphur is therefore well integrated in the porous structure, as it was encapsulated into the narrow micropores of carbon spheres by thermal treatment. It is also found the potential plateau at 2.4 V (vs. Li^+/Li) does not disappear completely after the first few cycles, further confirming the effectiveness of melt infusion to better retain sulphur onto the carbon spheres. Additionally, it is believed that the electrochemical reaction of the sulphur cathode is constrained inside the narrow micropores of carbon and correspondingly higher capacity values can be obtained. The rGO@MI_CS, in which the composite material is wrapped by rGO, shows excellent electrochemical performances (**Fig. 7 c**). In principle, a direct wrapping of S particles could lead to improved sulphur cathode material. Melt diffusion of S is widely used to prepare C/S composite taking the advantage that the conductive network of graphene can contact sulfur particles in "plane-to-point" mode. However, polysulphides formed during discharge can still readily diffuse out of graphene sheets with related "shuttle" effects. Thus, it is important to obtain sulphur particles well coated and confined. The sulphur dual confinement approach here proposed, with both MPC and rGO, helps minimize the dissolution and diffusion of polysulfides, decrease shuttle effects and accommodate volume expansions during discharge [39]. These factors have relevance on the performance of rGO@MI_CS cathode, being the first discharge capacity of 1103 mA h g^{-1} (**Fig. 7 c**). On the second cycle, the discharge capacity decreases to 897 mA h g^{-1}, with capacity retention of 81 % after SEI layer formation. S utilization is higher despite the lower S content in rGO@MI_CS compared to MI_CS. At the 5th cycle at 0.1 C the discharge capacity is still 760 mA h g^{-1}.

As **Fig. 7 d** is concerned, recent progress on sulphur cell design underlined that inserting a carbon interlayer between the cathode and separator is an effective way to protect cathode and anode simultaneously. Different carbon modified multifunctional separators able to act as interlayers to trap/block polysulphides and limiting parasitic reactions have been proposed [40, 41].

The positive effect of an interlayer is weaken polysulphides shuttle effect at the lithium anode, suggesting that most of polysulphides can be trapped between the interlayer and cathode, and even oxidized to S_8/Li_2S_8. The interlayer has no adverse effect on the cathode but enhances the electrochemical stability of the cell [42]. It is worth noted, however, that the interlayer system is inert overweight, which needs to be lightened as much as possible, but thicker interlayers are preferred in case of cathodes with high sulfur areal loading amount. Additionally, the application of interlayers require easy fabrication, compatibility with cell assembly processes and low cost. Here we can show that major improvements of the electrochemical performance are achieved with commercially available porous carbon papers as interlayers. The results are shown in **Fig. 7 d**. In this case, the rGO@MI_CS cathode material is coupled with carbon fibre paper in place of glass fibre separator. rGO@MI_CS_CFP showed excellent capacity retention, being the first discharge capacity of 1108 mA h g^{-1} and of 947 mA h g^{-1} on the second cycle at C/10. This high capacity retention could be linked to suppression of PS from composite surfaces at cathode side by the carbon fibre separator. The benefits due to the use of the interlayer are evident by comparing the discharge capacities of the cathodes at two different C rates (**Table 2**). The comparison between rGO@MI_CS_GF and rGO@MI_CS_CFP shows that their initial performance are similar, demonstrating 1103 mA h g^{-1} and 1108 mA h g^{-1} at C/10, respectively. However, the discharge capacity after 100 cycles at C/5 is significantly lower for rGO@MI_CS_GF resulting in 483 mA h g^{-1} compared to 723 mA h g^{-1} of rGO@MI_CS_CFP with the interlayer.

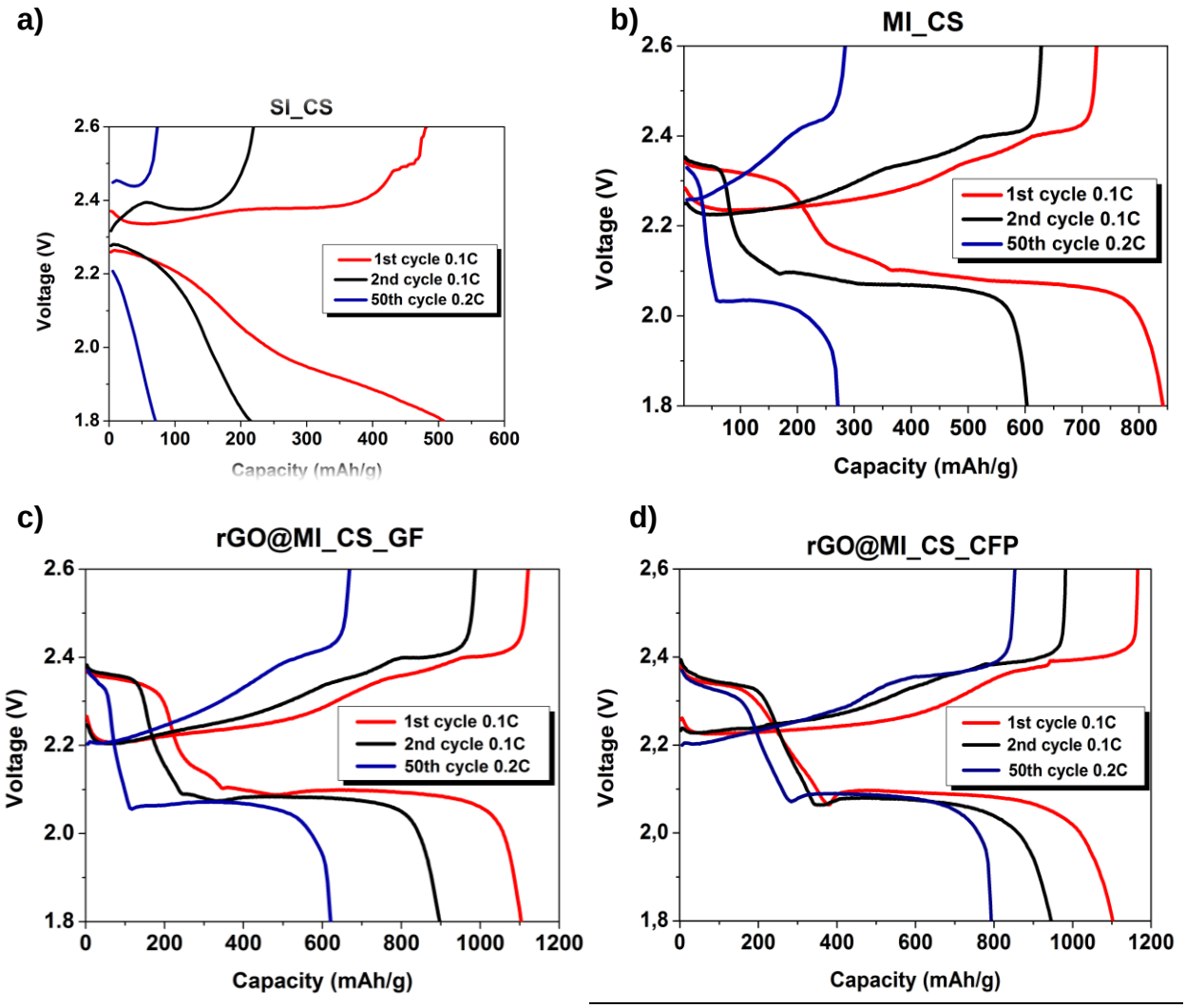

Figure 7: Charge and discharge capacity of a) SI_CS b) MI_CS c) rGO@MI_CS with GF d) rGO@MI_CS with CFP for the first two cycles at 0.1C

Table 2: Discharge capacities of C/S composites reported for different cycles with different C-rate

Discharge Capacity	SI_CS	MI_CS	rGO@MI_CS_GF	rGO@MI_CS_CFP
1st cycle at C/10	508.25	841.89	1103.01	1108.10
2nd cycle at C/10	214.72	603.09	897.04	946.95
5th cycle at C/10	157.89	447.06	746.87	909.37
6th cycle at C/5	92.90	342.24	626.05	846.82

10th cycle at C/5	95.66	298.39	547.50	839.36
50th cycle at C/5	70.11	271.01	621.48	808.61
100th cycle at C/5	49.23	203.43	482.97	722.71

Next, cycling performance of the three Li−S cells was studied (**Fig. 8**). At a rate of 0.2 C, an initial capacity of about 100 mA h g^{-1} was measured for SI_CS, followed by a decrease to relatively stable capacity of 70 mA h g^{-1} after 50 continuous cycles. Although 96 % coulombic efficiency, within the next 50 cycles the capacity dropped to 50 mA h g^{-1} indicating the poor performances of SI_CS cathode. For the other two other cathodes, higher capacity was observed. For MI_CS, about 0.40 % decrease in the capacity from the first to the 100th cycle at the same rate of 0.2 C was noted (**Fig. 8 b**). At the end of the cycling test, the discharge capacity remained at about 200 mA h g^{-1} based on the mass of sulphur. As for the rGO@MI_CS, better cycling performance was achieved (**Fig. 8 c**) with 620 mA h g^{-1} at 50th cycle. The initial capacity increase observed for rGO@MI_CS at 0.2 C can be probably assigned to the activation of high-loading active material [43]. Similar capacity trends have already been observed and reported in literature [44]. Initial lower values of capacity can also be due to incomplete soaking of the S cathode by the electrolyte. The rGO@MI_CS cathode with carbon paper interlayer (**Fig. 8 d**) showed excellent performance for prolonged cycling at 0.2 C. Cell with this configuration showed 850 mA h g^{-1} capacity that is stable for more than 100 cycles with about 0.1 % capacity loss per cycle. For the rate capability shown in **Fig. 9**, the rGO@MI_CS electrode with carbon paper interlayer delivered superior rate capability of more than 450 mA h g^{-1} at 1C. In addition, the electrode at different rates exhibited good capacity recovery (from about 800 mA h g^{-1} at 0.2 C to 600 mA h g^{-1} at 0.5 C and then back to 800 mA h g^{-1}), indicating its high reversibility. Once again, this proves the complexity of the lithium-sulfur system and the need to combine efficient cathodes with parallel efforts devoted to hinder the shuttling of polysulphides inside the cell.

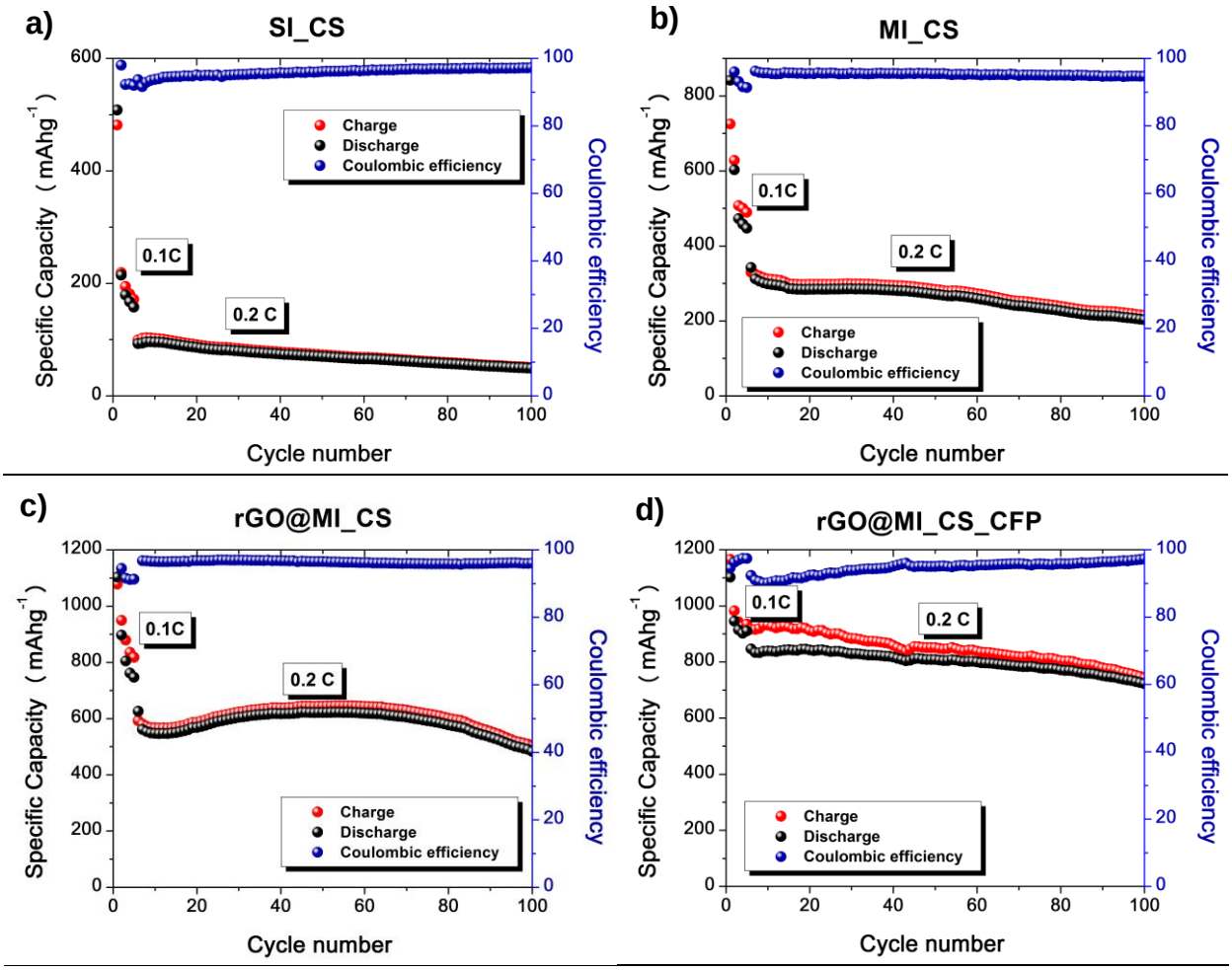

Figure 8: Long-term Galvanostatic cycling at 0.2C and Coulombic efficiencies of a) SI_CS b) MI_CS c) rGO@MI_CS with GF d) rGO@MI_CS with CFP

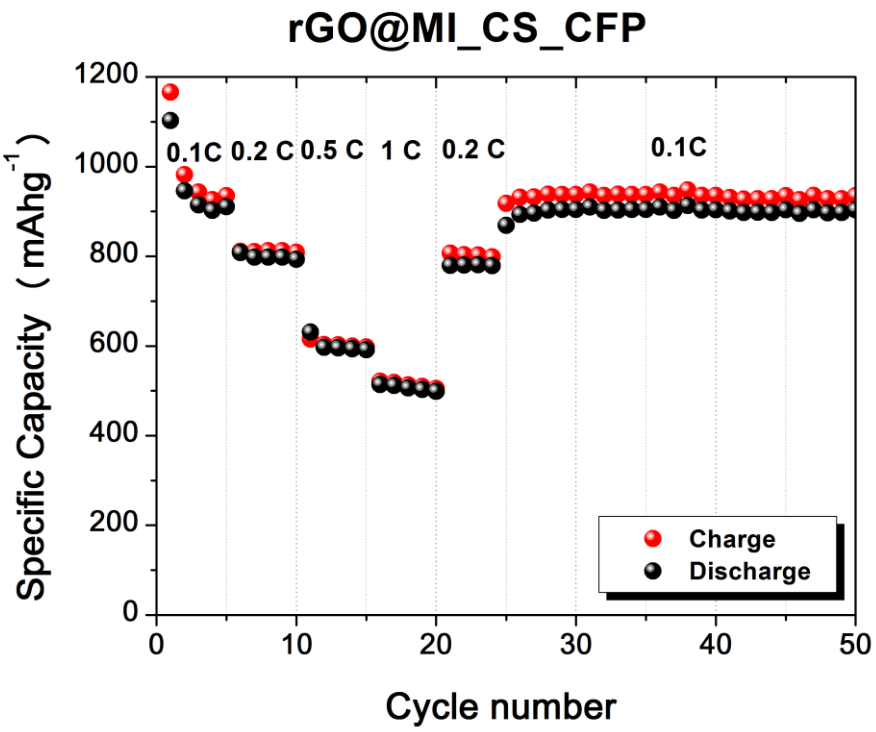

Figure 9: Rate capability of rGO@MI_CS composite with CFP as interlayer.

4. Conclusions

In summary, we have proposed a novel carbon matrix derived from bio-based material to host sulphur for Li-S battery application. For the first time it was successfully demonstrated that microporous carbons can be obtained from pyrolysis of polymer β-cyclodextrin and exhibited a spongy structure that makes them absorptive for sulphur. The overall carbon preparation process is easy to scale-up and forecasts new strategies for microporous carbon preparation. The MPC serves as a host for encapsulated chainlike sulphur and probably to confine polysulphides. We have demonstrated that to make S and Li_2S available for electrochemical process, it is necessary to provide a suitable conductive network by rGO wrapping the C/S composite. By using the proposed strategy, we are able to reach 1108 mA h g^{-1} at C/10 and 626 mA h g^{-1} at C/5 with capacity loss of 0.11 % per cycle for more than 100 cycles. Dual layer cathode protection strategy could prove a step forward towards commercial Li/S batteries for EVs using MPCs.

Acknowledgments

Financial support was provided by the European Union H2020 NMP-17-2014 ALISE (GA 666157). The authors sincerely thank Mr. Mauro Raimondo for FESEM analyses.

Figure Captions

Scheme 1 Schematic representation of the opted strategy to prepare rGO wrapped functional microporous C/S composites.

Scheme 2 Schematic illustration of the production steps to prepare rGO functional microporous C/S composites.

Fig. 1 FESEM images of MPC prepared from β-cyclodextrin nanosponge.

Fig. 2 SEM images of **a)** SI_CS **b)** MI_CS **c)** rGO@MI_CS (images are at different scale to observe the typical structures present in the composites).

Fig. 3 Secondary image and back-scattered contrast of carbon and sulfur **a)** SI_CS **b)** MI_CS **c)** rGO@MI_CS.

Fig. 4 Sulphur mapping in C/S composites using EDS analysis for **a)** SI_CS **b)** MI_CS **c)** rGO@MI_CS.

Fig. 5 Isotherms from BET analysis of a) MPC b) SI_CS c) MI_CS d) rGO@MI_CS.

Fig. 6 a) XRD analysis of sulphur, carbon and carbon sulphur composite; **b)** illustration of sulphur distribution in rGO wrapped microporous carbon from the characteristics EDS, XRD and BET results.

Fig. 7 Charge and discharge capacity of **a)** SI_CS **b)** MI_CS **c)** rGO@MI_CS with GF **d)** rGO@MI_CS with CFP for the first two cycles at 0.1C.

Fig. 8 Long-term Galvanostatic cycling at 0.2C and Coulombic efficiencies of **a)** SI_CS **b)** MI_CS **c)** rGO@MI_CS with GF **d)** rGO@MI_CS with CFP.

Fig. 9 Rate capability of rGO@MI_CS composite with CFP as interlayer.

Table Captions

Table 1 Elemental analysis of MPC and C/S composites.

Table 2 Discharge capacities of C/S composites reported for different cycles with different C-rate.

References

[1] Manthiram A, Chung SH, Zu CX (2015) Advanced Materials 27(12):1980-2006.
[2] Bruce PG, Freunberger SA, Hardwick LJ, Tarascon J-M (2012) Nat Mater 11:19-29.
[3] Evers S, Nazar LF (2013) Acc Chem Res 46(5):1135–1143.
[4] Fang X, Peng HS (2015) Small 11(13):1488-1511.
[5] Ji X, Lee KT, Nazar LF (2009) Nat Mater 8(6):500-506.
[6] Niu S, Zhou G, Lv W, Shi H, Luo C, He Y, Li B, Yang Q-H, Kang F (2016) Carbon 109: 1-6.
[7] Xu Y, Wen Y, Zhu Y, Gaskell K, Cychosz K A, Eichhorn B, Xu K, Wang C (2015) Advanced Functional Materials 25(27):4312-4320.
[8] Zhang B, Qin X, Li GR, Gao XP (2010) Energy Environ Sci 3(10):1531-1537.
[9] Tao X, Chen X, Xia Y, Huang H, Gan Y, Wu R, Chen F, Zhang W (2013) J Mater Chem A 1(10):3295-3301.
[10] Jayaprakash N, Shen J, Moganty SS, Corona A, Archer LA (2011) Angew Chem Int Ed Engl 50(26):5904-5908.
[11] Zhang C, Lin Y, Liu J (2015) J Mater Chem A 3(20):10760-10766.
[12] Xin S, Gu Lin, Zhao N-H, Yin Y-X, Zhou L-J, Guo Y-G, Wan L-J (2012) J Am Chem Soc 134(45):18510-18513.
[13] Yuan G, Wang, Wang H, Bai J (2015) J Nanopart Res17:36.
[14] Zhang Z, Li Q, Zhang K, Lai Y, Li J (2015) Electrochimica Acta 152:53-60.
[15] Zhou GM, Zhao YB, Manthiram A (2015) Adv Energy Mater 5(9):1402263.
[16] Sun L, Kong W, Jiang Y, Wu H, Jiang K, Wang J, Fan S (2015) J Mater Chem A 3(10): 5305-5312.
[17] Zhang L, Huang H, Yin H, Xia Y, Luo J, Liang C, Gan Y, Tao X, Zhang W (2015) J Mater Chem A 3(32):16513-16519.
[18] Chen L, Shaw LL (2014) J Power Sources 267:770-783.
[19] Zhao XY, Tu JP, Lu Y, Cai JB, Zhang YJ, Wang XL, Gu CD (2013) Electrochimica Acta 113:256-262.
[20] Li Z, Huang Y, Yuan L, Hao Z, Huang Y (2015) Carbon 92:41-63.
[21] Li Z, Yuan L, Yi Z, Sun Y, Liu Y, Jiang Y, Shen Y, Xin Y, Zhang Z, Huang Y (2014) Adv Energy Mater 4(7):1301473.
[22] Markevich E, Salitra G, Talyosef Y, Chesneau F, Aurbach D (2017) J Electrochem Soc 164 (1):A6244-A6253.
[23] Wu HB, Wei S, Zhang L, Xu R, Hng HH, Lou X W (2013) Chemistry 19(33):10804-10808.

[24] Lee J, Kim J, Hyeon T (2006) Adv Mater 18(16):2073-2094.
[25] Ryu HS, Park J W, Park J, Ahn J-P, Kim K-W, Ahn J-H, Nam T-H, Wangad G, Ahn H-J (2013) J Mater Chem A 1(5):1573-1578.
[26] Wang J, Yue K, Zhu X,. Wang KL, Duan L (2016) Phys Chem Chem Phys 18:261-266.
[27] Jin KK, Zhou XF, Liu ZP (2015) Nanomaterials 5(3):1481-1492.
[28] Ji X, Lee KT, Nazar LF (2009) Nat Mater 8:500-506.
[29] Wun S, Ge R, Lu M, Xu R, Zhang Z (2015) Nano Energy 15:379–405.
[30] Zanetti M, Anceschia A, Magnacca G, Spezzati G, Caldera F, Rosi G P, Trotta F (2016) Microporous and Mesoporous Materials 235:178-184.
[31] Trotta F, Caldera F, Zanetti M, Anceschi A, Magnacca G (2014) Patent US20160271580 A1.
[32] Steijns M, Mars P (1976) J Colloid and Interface Sci 57(1):175-180.
[33] Meyer B (1976) Chem Rev 76(3):367-388.
[34] Theilig E (1982) NASA Contractor Report 3594 NASA Office of Space Science and Applications under Grant NAGW-132:13.
[35] Wong MW (2003) R. Steudel, Editor, Springer Berlin Heidelberg: Berlin, Heidelberg:1-30.
[36] Konios D, Stylianakis MM, Stratakis E, Kymakis E (2014) J Colloid Interface Science 430:108–112.
[37] Zhang B, Qin X, Li GR, Gao XP (2010) Energy Environ Sci 3:1531–1537.
[38] Liang C, Dudney N J, Howe JY (2009) Chem Mater 21(19):4724–4730.
[39] Yu M, Li R, Wu M, Shi G (2015) Energy Storage Materials 1:51–73.
[40] Chung SH, Manthiram A (2014) Adv Funct Mater 24:5299–5306.
[41] Su Y-S, Manthiram A (2014) Nat Commun 3:1166.
[42] Kong L-L, Zhang Z, Zhang Y-Z, Liu S, Li G-R, Gao X-P (2016) ACS Appl. Mater. Interfaces 8(46):31684–31694.
[43] Chung S-H, Chang CH, Manthiram A (2016) ACS Nano10 (11):10462–10470.
[44] Chung SH, Chang CH, Manthiram A (2016) J. Power Sources 334:179−190.